Batbayar Khuyagbaatar
Department of Mechanical Engineering,
Kyung Hee University,
1 Seocheon-dong,
Giheung-gu,
Yongin-si, Gyeonggi-do 446-701, Korea
e-mail: bayaraa_3d@yahoo.com

Kyungsoo Kim
Department of Applied Mathematics,
Kyung Hee University,
1 Seocheon-dong,
Giheung-gu,
Yongin-si, Gyeonggi-do 446-701, Korea
e-mail: kyungsoo@khu.ac.kr

Won Man Park
Department of Mechanical Engineering,
Kyung Hee University,
1 Seocheon-dong,
Giheung-gu,
Yongin-si, Gyeonggi-do 446-701, Korea
e-mail: muhaguy@hanmail.net

Yoon Hyuk Kim[1]
Department of Mechanical Engineering,
Kyung Hee University,
1 Seocheon-dong,
Giheung-gu,
Yongin-si, Gyeonggi-do 446-701, Korea
e-mail: yoonhkim@khu.ac.kr

Biomechanical Behaviors in Three Types of Spinal Cord Injury Mechanisms

Clinically, spinal cord injuries (SCIs) are radiographically evaluated and diagnosed from plain radiographs, computed tomography (CT), and magnetic resonance imaging. However, it is difficult to conclude that radiographic evaluation of SCI can directly explain the fundamental mechanism of spinal cord damage. The von-Mises stress and maximum principal strain are directly associated with neurological damage in the spinal cord from a biomechanical viewpoint. In this study, the von-Mises stress and maximum principal strain in the spinal cord as well as the cord cross-sectional area (CSA) were analyzed under various magnitudes for contusion, dislocation, and distraction SCI mechanisms, using a finite-element (FE) model of the cervical spine with spinal cord including white matter, gray matter, dura mater with nerve roots, and cerebrospinal fluid (CSF). A regression analysis was performed to find correlation between peak von-Mises stress/peak maximum principal strain at the cross section of the highest reduction in CSA and corresponding reduction in CSA of the cord. Dislocation and contusion showed greater peak stress and strain values in the cord than distraction. The substantial increases in von-Mises stress as well as CSA reduction similar to or more than 30% were produced at a 60% contusion and a 60% dislocation, while the maximum principal strain was gradually increased as injury severity elevated. In addition, the CSA reduction had a strong correlation with peak von-Mises stress/peak maximum principal strain for the three injury mechanisms, which might be fundamental information in elucidating the relationship between radiographic and mechanical parameters related to SCI.
[DOI: 10.1115/1.4033794]

Introduction

Acute SCI has been widely investigated because of its clinical importance [1]. Vertebral dislocation represents a pattern of injury to the spinal column that often results in a SCI and this type of column injury results in a dislocation or shear mechanism of injury to the spinal cord. Similarly, a burst fracture is a common column injury pattern that often results in a contusion injury mechanism to the spinal cord. In addition, spinal distraction frequently contributes to neurological deficits and SCI that stretches the spinal cord [1–4]. These distinct injury mechanisms produce varying patterns of primary spinal cord damage in experimental models [4,5], and increasing injury severity results in a graded increase in the extent of spinal cord damage [6].

Clinically, SCIs are radiographically evaluated and diagnosed using the spinal cord diameter, the spinal canal diameter, and the Pavlov ratio (the ratio of the sagittal diameter of the cervical canal to the corresponding diameter of the vertebral body) from plain radiographs as well as the CSAs of the spinal cord and spinal canal from CT or magnetic resonance imaging. A Pavlov ratio less than a threshold (e.g., 0.8) is considered poor clinical outcomes [7,8]. Moreover, there have been several studies regarding the relationship between the reduction in CSA of the spinal cord or spinal canal and the severity of neurological damage. A 30% reduction in spinal cord CSA was correlated to neurological deficits, while a 40–65% reduction was associated with severe injuries [9–12]. The CSA of the spinal cord at the level of maximum compression was closely correlated with the severity of myelopathy [13]. However, it is difficult to conclude that radiographic evaluation of SCI can directly explain the fundamental mechanism of spinal cord damage, even though it can be used to diagnose the severity of SCI.

From a biomechanical viewpoint, the von-Mises stress and maximum principal strain are directly associated with neurological damage in the spinal cord [14–17]. The maximum principal strain was reported as a good predictor of neural tissue damage by both in vivo and computational studies [14–16]. The von-Mises stress was also correlated with neurological deficits and damage in the spinal cord [17]. Due to the limitations of experimental observation of stress and strain related to SCIs, FE analysis has been used to understand SCI mechanisms by investigating the relationship between biomechanical parameters (e.g., stress and strain) and neurological deficits and damage. The stress and strain causing SCIs were analyzed in simple cases [18], contusion injuries [15,19,20], and various spinal column injury patterns [21] using FE models. Moreover, the strain distributions in the cord during contusion and dislocation mechanisms were simulated using FE models of rat cervical spine [16]. However, few studies have performed an overall comparison between the stress and strain in the spinal cord and the CSA during distinct injury mechanisms. Further, the correlation between CSA reduction and stress/strain could explain relationship between radiographic and mechanical parameters related to SCIs.

In this study, we analyzed the von-Mises stress and maximum principal strain in the spinal cord as well as the cord CSA for SCIs by contusion, dislocation, and distraction with various degrees of injury severity, using an FE model of the cervical spine with spinal cord including white matter, gray matter, dura mater with nerve roots, and CSF. The injury severity of each SCI was decided based on clinical studies. We then quantified the

[1]Corresponding author.
Manuscript received August 3, 2015; final manuscript received June 1, 2016; published online June 22, 2016. Assoc. Editor: Brian D. Stemper.

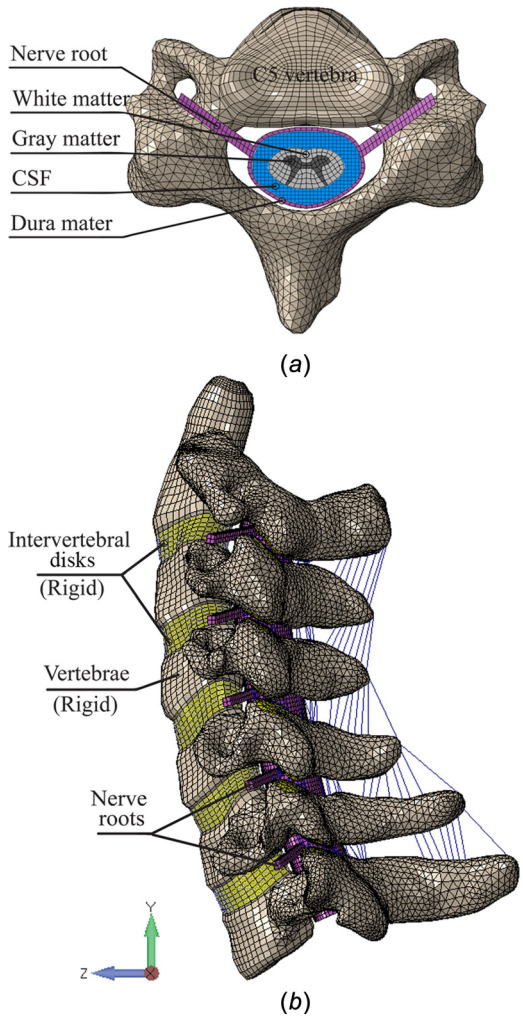

Fig. 1 The FE model of the cervical spine with the spinal cord: (*a*) axial view (*b*) and sagittal view. The cervical spine components, including vertebrae and intervertebral disks, were modeled as rigid bodies.

relationship between peak von-Mises stress/peak maximum principal strain at the cross section of the highest reduction in CSA and corresponding reduction in CSA of the cord.

Material and Methods

A three-dimensional FE model of the human C2–C7 cervical spine with the spinal cord was developed based on our previously validated models [20,22]. The geometry of the cervical spine was obtained from the CT images of C2–C7 at 1 mm intervals in a 175 cm tall 21-year old man. The geometry of the spinal cord was based on the geometry of the cervical column with quantitative measurements of the human spinal cord [23,24]. The reconstructed spinal cord model consisted of white matter, gray matter, dura mater with nerve roots, and a CSF layer, and it was assumed to be symmetrical about the midsagittal plane (Fig. 1). The dural sheath was placed 2.5 mm from the cord, since the thickness of the CSF layer in the human cervical spine was 1.5 mm to 4.0 mm in an experimental study [25]. The FE model was then developed with 103,532 nodes and 201,282 elements, excluding fluid elements. Hexahedral elements were used and their skewness, warpage, and aspect ratio were below 0.20, 0.0005, and 1.71, respectively. Fluid elements were modeled as Eulerian elements, which are an arbitrary collection of cubic elements that fully encompass the region of fluid material during the analysis. The volume between the dural sheath and the cord was filled with the Eulerian material defined by the Eulerian volume fraction. The interaction between the fluid material and solid bodies was then coupled by the Eulerian–Lagrangian analysis technique using ABAQUS/EXPLICIT (ABAQUS™, ABAQUS Inc., Providence, RI). Furthermore, the cervical spine components, including vertebrae and intervertebral disks, were modeled as rigid bodies to reduce computational cost.

Material properties of the spinal cord, such as the stress–strain curve of the white and gray matter, were obtained from an experimental study [26]. Ogden's nonlinear, hyperelastic constitutive model using a first-order strain energy function was utilized for the white and gray matter [27]. The dura mater with nerve roots were assumed to be a single tangent modulus, as derived previously [28]. Material properties of the CSF were demonstrated with a Newtonian fluid characterized by the viscosity of CSF [29,30]. The material properties used in the spinal cord model are summarized in Table 1.

To validate the developed model, a dynamic contusion impact on the spinal cord using three types of pellets was simulated as described previously [20]. The cylindrical shaped pellets were

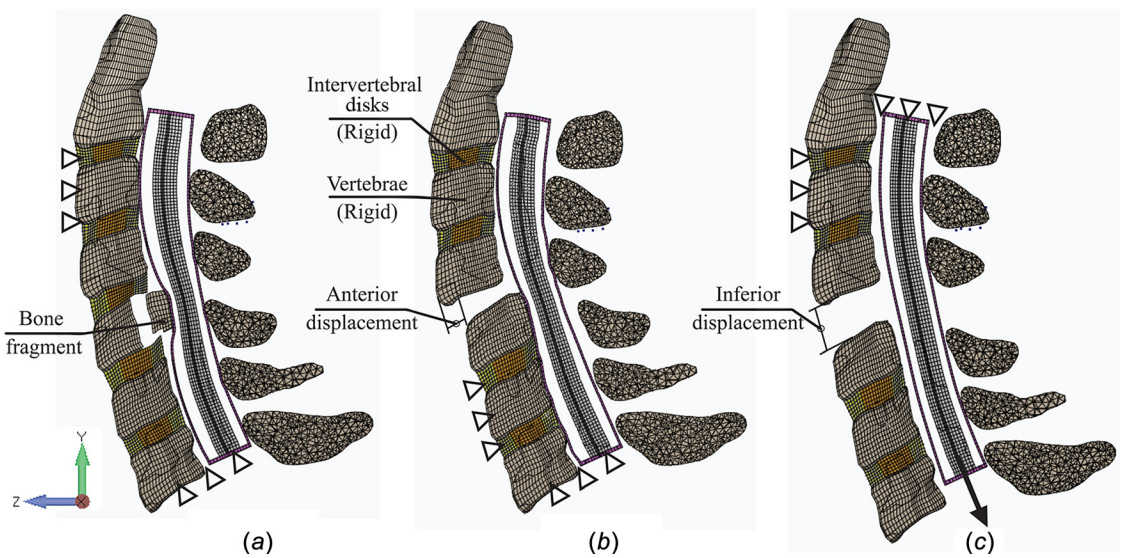

Fig. 2 FE models for (*a*) contusion injury, (*b*) dislocation injury, and (*c*) distraction injury

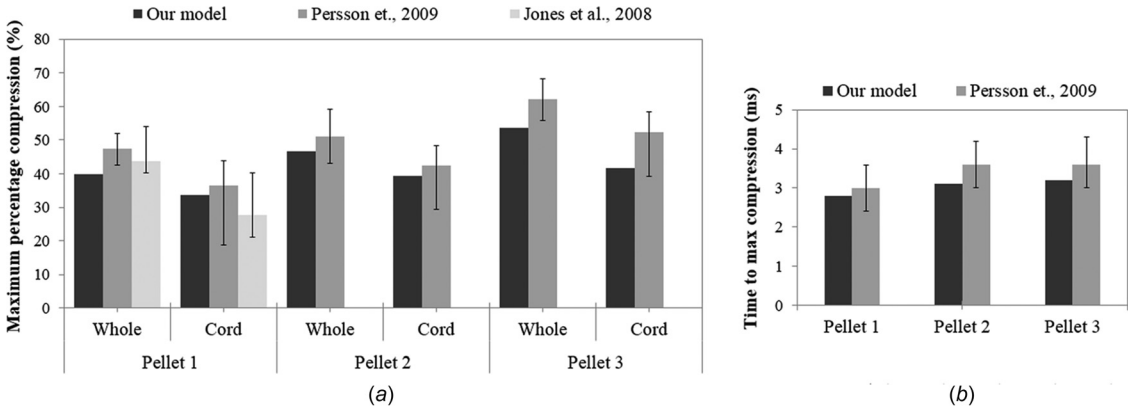

Fig. 3 (*a*) Comparison of maximum percentage compression of the whole spinal cord and the cord within the dural sheath for our FE results and previous experimental studies [32,33] and (*b*) comparison of time to maximum compression of the whole spinal cord between our FE results and a previous experimental study [33]. The pellets have same mass and different impact areas (pellet 1: 314 mm^2; pellet 2: 157 mm^2; and pellet 3: 78.5 mm^2).

used in the impacts, where the pellets were modeled with the same mass (7 g) and different impact areas (pellet 1: 314 mm^2 with the diameter of 20 mm; pellet 2: 157 mm^2 with the diameter of 14.14 mm; pellet 3: 78.5 mm^2 with the diameter of 10 mm). In order to simulate the impact on the spinal cord, the elements of the lamina and spinous processes of the middle vertebrae (C4 and C5) were removed. The pellets were free only in the perpendicular direction to the spinal cord surface, and the initial impact velocity was assumed to be 4.5 m/s based on a simulated burst fracture [31]. The vertebral bodies, bottom of the spinal cord, and distal nodes of nerve roots were fixed in all directions. The displacement behavior of the spinal cord such as maximum percentage compression of the whole spinal cord and the cord within the dural sheath in the anterior–posterior direction was measured from each impact and then compared to those reported in previous ex vivo experimental studies [32,33]. In addition, the time to maximum compression of the whole spinal cord was compared to previous experimental results [33].

For contusion injury, we simulated the contusion of the bone fragment from the vertebral body onto the spinal canal. All vertebrae, the bottom nodes of the spinal cord, and the distal nodes of the nerve roots were constrained. The bone fragment was the posterior one-third of the C5 vertebral body with impact area about 120 mm^2, and it was enforced by applying 20%, 30%, 40%, 50%, or 60% of the anterior–posterior diameter of the spinal canal at the C5 level, based on previous studies [31,34] (Fig. 2(*a*)). The maximum canal reduction of 60% was decided based on radiographic findings showing that reduction in the spinal canal by more than 50% resulted in spinal cord trauma [35,36].

For dislocation injury, the facet joints and discoligamentous complex (DLC) between C4 and C5 were removed. The bottom nodes of the spinal cord, the distal nodes of the nerve roots from C5 to C7, and the C5 to C7 vertebrae were constrained. The C2 to C4 vertebrae were anteriorly displaced by 20%, 30%, 40%, 50%, or 60% of the anterior–posterior diameter of the C4 vertebral body (Fig. 2(*b*)). The maximum anterior displacement of 60% was selected because radiographic measurements showed that a mean gross anterior displacement of 55% (range, 35–75%) of the anterior–posterior diameter of the corresponding vertebral body along with contralateral facet joint dislocation could cause severe neurological deficits [37].

For distraction injury, the facet joints and DLC between C4 and C5 were also removed. The top nodes of the spinal cord and the distal nodes of the nerve roots from C2 to C4 vertebrae, and the C2 to C4 vertebrae were constrained. The C5 to C7 vertebrae were displaced downward by 3 mm, 6 mm, 9 mm, 12 mm, or 15 mm (Fig. 2(*c*)). The maximum displacement of 15 mm was chosen because the strain at this displacement exceeded the experimentally observed failure tensile strain, 0.16, of the cervical spine cord [38]. Displacement of the vertebral body and spinal cord were not equal since they were not rigidly linked. Thus, the coupling ratio of 0.55, which was defined by the ratio of spinal cord strain to vertebral column strain, was considered based on a study that utilized a nonhuman primate model to determine the coupling relationship between the spinal cord strain and the vertebral column strain [39]. The displacement rates for the three types of injuries were about 100 cm/s, which was same to that used in the experimental SCI devices [40].

All SCI simulations were based on an experimental study [40] and the subaxial cervical spine injury classification system [41]. Friction was not included, as a previous study reported that the frictional coefficient had little influence on stress and strain distributions [15]. The peak von-Mises stress and peak maximum principal strain in the spinal cord and the reduction in cord CSA were estimated for three injury mechanisms (contusion, dislocation, and distraction) using FE analysis (ABAQUS™, ABAQUS Inc., Providence, RI) at each level of injury severity. Then, the peak values of stress and strain and CSA reduction were analyzed. The convergence of FE analysis was guaranteed based on our previous study [20]. Regression analysis with power functions was performed to quantify relationships between peak stress and peak strain and the CSA reduction at the same cross section of the spinal cord for distinct injury mechanisms.

Results

The FE model was validated by comparing the maximum percentage compression of the whole spinal cord and the cord within

Table 1 Material properties used for FE model of the spinal cord

	Material properties	Density	References
White matter	Hyperelastic (Ogden): $\mu = 4.0$ kPa, $\alpha = 12.5$	1050 kg/m^3	[26,27]
Gray matter	Hyperelastic (Ogden): $\mu = 4.1$ kPa, $\alpha = 14.7$	1050 kg/m^3	[26]
Dura mater (nerve roots)	Elastic modulus: 80 MPa Poisson's ratio: 0.49	1000 kg/m^3	[28]
CSF	Viscosity (Newtonian): 0.001 Pa·s	1000 kg/m^3	[29,30]

the dural sheath from the dynamic contusion impacts using three types of pellets with previous ex vivo experimental studies. The maximum percentage compression of the whole spinal cord and the cord within the dural sheath at a velocity of 4.5 m/s was 40% and 34% for pellet 1, 47% and 40% for pellet 2, and 54% and 42% for pellet 3, respectively. These values were consistent with previous experimental results [32,33] (Fig. 3(*a*)). In addition, the FE model showed similar trend of time to maximum compression of the whole spinal cord with previous experimental study [33]. The time to maximum compression of the whole spinal cord ranged from 2.8 ms to 3.2 ms for the three types of pellets (Fig. 3(*b*)), which were comparable to previously reported times of 3.0 ms to 3.6 ms [33].

The von-Mises stress distributions in the transverse and sagittal cross sections of the deformed spinal cord are presented in Fig. 4(*a*). The peak stresses occurred in the outer part of the gray matter in contusion and dislocation injuries and in all the gray matter in distraction injury at the cross section of the highest reduction in CSA. In both the contusion and dislocation, the maximum stresses were gradually elevated from 20% to 50%, but they substantially increased at 60%. Contusion and dislocation produced greater stress values (0.125 MPa in contusion and 0.328 MPa in dislocation) than distraction (0.018 MPa) (Fig. 5(*a*)).

The maximum principal strain distributions in the transverse and sagittal cross sections of the deformed spinal cord are shown in Fig. 4(*b*). The strain distributions were similar to the stress distributions. Peak strains were located at the outer part of the gray matter in contusion and dislocation, while distraction produced uniform cord strain. The maximum principal strains were 0.39 in contusion, 0.44 in dislocation, and 0.21 in distraction (Fig. 5(*b*)). The maximum cord strains increased proportionally to the injury severity for all injury mechanisms.

The CSAs were gradually reduced in all three mechanisms as the injury severity increased (Fig. 5(*c*)). The CSAs decreased by 27.5%, 34.5%, and 19.3% compared to the intact area during maximum contusion (60%), dislocation (60%), and distraction (15 mm). In the maximal contusion and dislocation cases, the reductions in CSA reached or exceeded 30% of the intact area. Regression analysis with power functions showed that CSA reduction strongly correlated with increasing peak von-Mises stress ($R^2 = 0.99$) and peak maximum principal strain ($R^2 = 0.90$) for three common SCI mechanisms (Fig. 6).

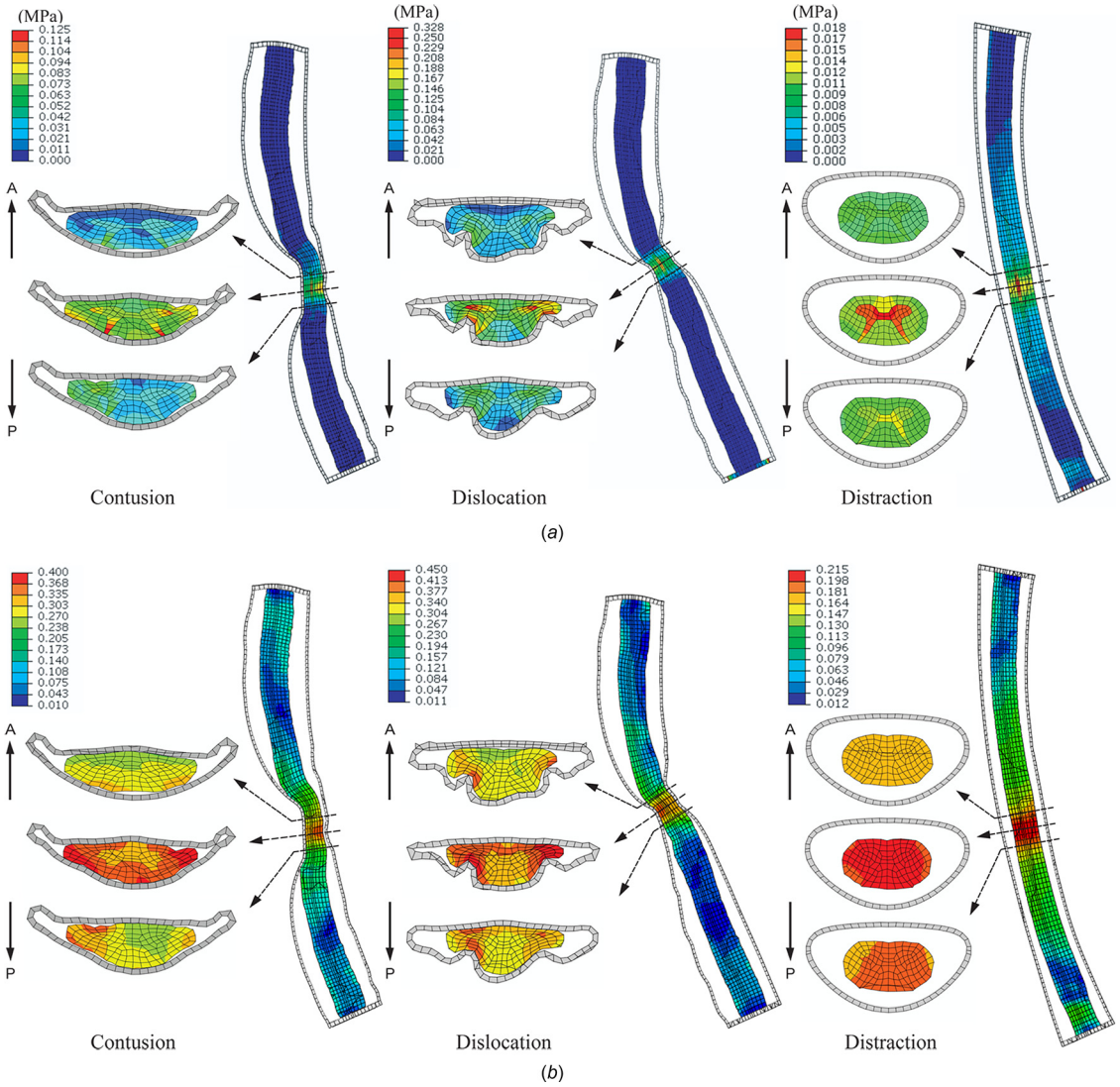

Fig. 4 (*a*) von-Mises stress in the cord for a 60% spinal canal reduction in contusion, a 60% anterior displacement in dislocation, and a 15 mm inferior displacement in distraction; (*b*) maximum principal strain in the cord for a 60% of spinal canal reduction in contusion, a 60% anterior displacement in dislocation, and a 15 mm inferior displacement in distraction. The "A" arrow indicates the anterior direction, while the "P" arrow indicates the posterior direction.

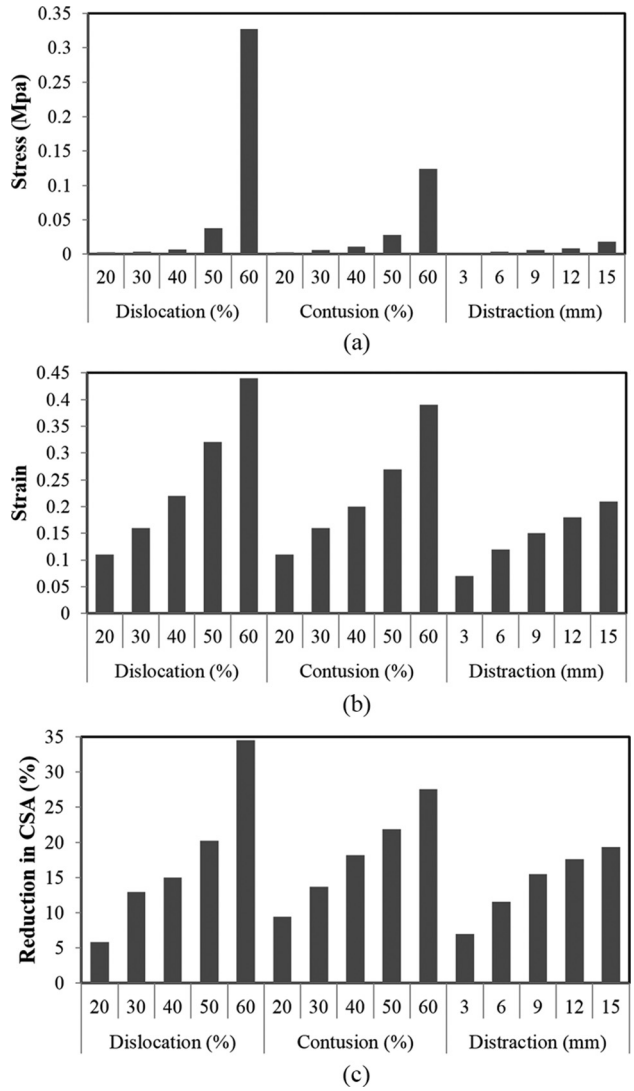

Fig. 5 (*a*) Maximum stress in the cord, (*b*) maximum principal strain in the cord, and (*c*) reduction in the cord CSA for each injury mechanisms

Discussion

The developed FE model of the cervical spine with the spinal cord was validated by the dynamic impact test on the spinal cord using three types of pellets, which was performed as in our previous study [20]. The maximum percentage compression of the whole spinal cord and the cord within the dural sheath as well as the time to maximum compression of the whole spinal cord were consistent with experimental studies [32,33]. Although the experimental studies used the bovine spinal cord and there were some disparities, the comparison is reasonable due to a number of anatomical and mechanical similarities between bovine and human cords [42]. In addition to the validation of the model, we validated the model for one specific situation against an experimental animal study [32,33], since there are few studies regarding mechanical and physical properties of the human spinal cord.

In this study, we investigated the von-Mises stress and maximum principal strain in the spinal cord as well as the reduction in cord CSA based on the injury severity for distinct injury mechanisms. Contusion and dislocation showed greater stresses and strains in the cord than distraction, whereas dislocation had slightly higher values than contusion**.** In the stress and strain distributions, the higher value regions in contusion and dislocation were located in the gray matter, while the relatively lower stress and strain were uniformly distributed in the gray matter (stress) and in the cord (strain) in distraction. These results were consistent with previous studies. Dislocation injury resulted in more severe damage to the cord and greater peak cord strain [4,16,21]. It was reported that contusion and dislocation produced similar patterns of central hemorrhage in the gray matter, whereas no appreciable hemorrhage was observed following distraction [4]. A computational study showed that contusion and dislocation resulted in higher strains at the injury site, while distraction produced more evenly distributed strain along the cord [21]. In addition, the maximum strains were 0.39, 0.44, and 0.21 in contusion, dislocation, and distraction, respectively, while those values were 0.3 and 0.4 in contusion and dislocation, respectively, although the rodent spinal cord was used [16].

Our results indicated that the stress in the cord was suddenly elevated and the CSA was reduced by approximately 30% at a 60% canal reduction (contusion) and a 60% anterior dislocation, while distraction increased the stress in the cord gradually and showed the strain more than 0.20 at a 15 mm distraction. These results could be explained from a mechanical viewpoint as narrowing of the spinal canal above a certain threshold by contusion and dislocation might cause a substantial increase compared to distraction. These findings agreed with clinical observations. The reduction by more than 50% in the spinal canal diameter was correlated with spinal cord trauma [35,36]. The gross anterior displacement of contralateral dislocation of the facet joints with a mean value of 55% in the anterior–posterior diameter of the corresponding vertebral body could cause severe neurological deficits [37], and an articular apposition above 50% of vertebral body diameter could result in DLC disruption [41]. The failure tensile strain of the cervical spine cord was experimentally measured as

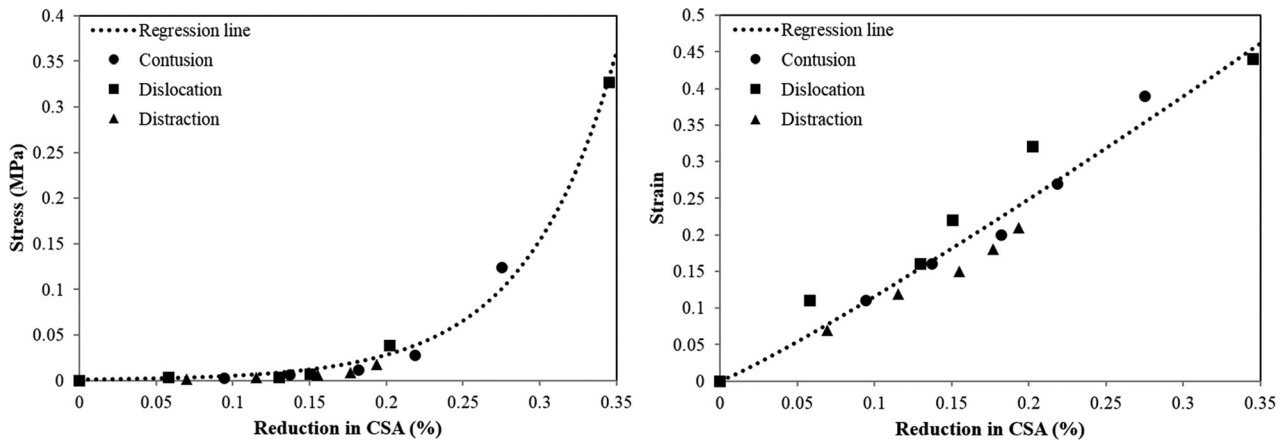

Fig. 6 Scatterplots of stress and strain versus reduction in CSA in all injury mechanisms

0.16 [38], though SCI may initiate with a strain of 0.1 [43]. A reduction in cord CSA by more than 30% was correlated with neurological deficits [9–12]. In the case of ossification of the posterior longitudinal ligament, a substantial increase of stress in the cord was observed above a threshold, such as a 60% spinal canal reduction [44].

Regression analysis results indicated that stress and strain might be converted from the CSA reduction due to the strong correlation both between stress and CSA reduction ($R^2 = 0.99$) and strain and CSA reduction ($R^2 = 0.90$). For example, a 20% CSA reduction corresponds to 0.030 MPa of stress and 0.249 of strain, while a 30% CSA reduction corresponds to 0.193 MPa of stress and 0.390 of strain. However, it should be noted that correlation established from only peak stress/peak strain that occurs at the cross section of the highest reduction in the CSA for each injury mechanisms and relations could be misused if the peak stress/peak strain and CSA values from different cross sections of the spinal cord. Also, the location of the damage to the spinal cord would have a significant effect on the neurological condition. Although radiographic parameters such as CSA reduction are conventionally used to diagnose SCI severity, the relationships between those parameters and mechanical parameters such as stress and strain, which are directly related to SCI, have been partly investigated in aforementioned experimental and clinical studies. This finding may be fundamental information to elucidate the relationship between radiographic and mechanical parameters related to SCI to explain why CSA reduction can be used as an indicator of SCI, even though this study was designed under simplified and ideal situations.

There were several limitations in this study. The model was validated only for the dynamic impact test against an experimental study without consideration for the dislocation or distraction injury conditions. Although the stress/strain distributions were compared with previous computational studies, the direct validation for stresses and strains within the spinal cord was not done. The stress/strain distributions may be highly dependent on the geometry of the vertebral fragments and impact velocities in the contusion mechanisms. Additional parameters, such as the impactor size and impact velocity, need to be considered to more thoroughly investigate the relationship between stress/strain and CSA reduction and to improve its confidence. In addition, there is a lack of information regarding quantitative correlation between the mechanical parameters (stress/strain) and neurological deficit in clinical condition.

Material properties were obtained from an experimental study [26], and separate stress–strain curves for white and gray matters using bovine spinal cord were considered, as in previous modeling studies [18,45,46], due to the lack of studies regarding material properties of human gray matter [47,48]. In addition, the constitutive model of the spinal cord was assumed. All vertebrae and intervertebral disks were modeled as rigid bodies to reduce computational costs, and thus an important boundary condition of the failed disk-vertebra interface in the dislocation case was not considered. The inward buckling of the dura mater occurred in the dislocation mechanism, even though it has not been observed experimentally. The flow of fluid initially located between the cord and the dural sheath was not incorporated since this had little effect on spinal cord deformation [19]. Finally, the cervical spine was modeled with one spinal alignment from one subject. Multiple cervical spine models with various spinal alignments using realistic patient-specific material properties as well as the sensitivity analysis for material properties can enhance the confidence of this study, although the results from this computational study are relevant to previous experimental and clinical studies.

In conclusion, we simulated three SCI mechanisms (contusion, dislocation, and distraction) based on clinical studies and analyzed the von-Mises stress and maximum principal strain in the spinal cord as well as the cord CSA for various injury severities. Dislocation and contusion showed greater stress and strain values in the cord than distraction. The substantial increases in cord stress as well as CSA reduction similar to or more than 30% were produced at a 60% contusion and a 60% dislocation, while the cord strain was gradually increased as injury severity elevated. In addition, the strong correlations between peak von-Mises stress/peak maximum principal strain and CSA reduction were quantified, which might be fundamental information in elucidating the relationship between radiographic and mechanical parameters related to SCI.

Acknowledgment

This research was supported by Sports Scientification of Convergent R&D Program through the National Research Foundation (NRF) of Korea funded by the Ministry of Science, ICT and Future Planning (NRF-2014M3C1B1033320).

Nomenclature

CSA = cross-sectional area
CSF = cerebrospinal fluid
CT = computed tomography
DLC = discoligamentous complex
FE = finite-element
SCI = spinal cord injury

References

[1] Sekhon, L. H., and Fehlings, M. G., 2001, "Epidemiology, Demographics, and Pathophysiology of Acute Spinal Cord Injury," Spine, **26**(24 Suppl.), pp. S2–S12.
[2] Maiman, D. J., Myklebust, J. B., Ho, K. C., and Coats, J., 1989, "Experimental Spinal Cord Injury Produced by Axial Tension," J. Spinal Disord., **2**(1), pp. 6–13.
[3] Dumont, R. J., Okonkwo, D. O., Verma, S., Hurlbert, R. J., Boulos, P. T., Ellegala, D. B., and Dumont, A. S., 2001, "Acute Spinal Cord Injury, Part I: Pathophysiologic Mechanisms," Clin. Neuropharmacol., **24**(5), pp. 254–264.
[4] Choo, A. M., Liu, J., Lam, C. K., Dvorak, M., Tetzlaff, W., and Oxland, T. R., 2007, "Contusion, Dislocation, and Distraction: Primary Hemorrhage and Membrane Permeability in Distinct Mechanisms of Spinal Cord Injury," J. Neurosurg. Spine, **6**(3), pp. 255–266.
[5] Clarke, E. C., Choo, A. M., Liu, J., Lam, C. K., Bilston, L. E., Tetzlaff, W., and Oxland, T. R., 2008, "Anterior Fracture-Dislocation is More Severe Than Lateral: A Biomechanical and Neuropathological Comparison in Rat Thoracolumbar Spine," J. Neurotrauma, **25**(4), pp. 371–383.
[6] Fiford, R. J., Bilston, L. E., Waite, P., and Lu, J., 2004, "A Vertebral Dislocation Model of Spinal Cord Injury in Rats," J. Neurotrauma, **21**(4), pp. 451–458.
[7] Bono, C. M., Vaccaro, A. R., Fehlings, M., Fisher, C., Dvorak, M., Ludwig, S., and Harrop, J., 2006, "Measurement Techniques for Lower Cervical Spine Injuries: Consensus Statement of the Spine Trauma Study Group," Spine, **31**(5), pp. 603–609.
[8] Song, K. J., Choi, B. W., Kim, S. J., Kim, G. H., Kim, Y. S., and Song, J. H., 2009, "The Relationship Between Spinal Stenosis and Neurological Outcome in Traumatic Cervical Spine Injury: An Analysis Using Pavlov's Ratio, Spinal Cord Area, and Spinal Canal Area," Clin. Orthop. Surg., **1**(1), pp. 11–18.
[9] Penning, L., Wilmink, J. T., van Woerden, H. H., and Knol, E., 1986, "CT Myelographic Findings in Degenerative Disorders of the Cervical Spine: Clinical Significance," Am. J. Roentgenol., **146**(4), pp. 793–801.
[10] Stevens, J. M., 1995, "Imaging of the Spinal Cord," J. Neurol., Neurosurg. Psychiatry, **58**(4), pp. 403–416.
[11] Fehlings, M. G., and Skaf, G., 1998, "A Review of the Pathophysiology of Cervical Spondylotic Myelopathy With Insights for Potential Novel Mechanisms Drawn From Traumatic Spinal Cord Injury," Spine, **23**(24), pp. 2730–2737.
[12] Kameyama, T., Hashizume, Y., Ando, T., Takahashi, A., Yanagi, T., and Mizuno, J., 1995, "Spinal Cord Morphology and Pathology in Ossification of the Posterior Longitudinal Ligament," Brain, **118**(Pt 1), pp. 263–278.
[13] Okada, Y., Ikada, T., Yamada, H., Sakamoto, R., and Katoh, S., 1993, "Magnetic Resonance Imaging Study on the Results of Surgery for Cervical Compression Myelopathy," Spine, **18**(14), pp. 2024–2029.
[14] Bain, A. C., and Meaney, D. F., 2000, "Tissue-Level Thresholds for Axonal Damage in an Experimental Model of Central Nervous System White Matter Injury," ASME J. Biomech. Eng., **122**(6), pp. 615–622.
[15] Maikos, J. T., Qian, Z., Metaxas, D., and Shreiber, D. I., 2008, "Finite Element Analysis of Spinal Cord Injury in the Rat," J. Neurotrauma, **25**(7), pp. 795–816.
[16] Russell, C. M., Choo, A. M., Tetzlaff, W., Chung, T. E., and Oxland, T. R., 2012, "Maximum Principal Strain Correlates With Spinal Cord Tissue Damage in Contusion and Dislocation Injuries in the Rat Cervical Spine," J. Neurotrauma, **29**(8), pp. 1574–1585.
[17] Ouyang, H., Galle, B., Li, J., Nauman, E., and Shi, R., 2008, "Biomechanics of Spinal Cord Injury: A Multimodal Investigation Using Ex Vivo Guinea Pig Spinal Cord White Matter," J. Neurotrauma, **25**(1), pp. 19–29.
[18] Li, X. F., and Dai, L. Y., 2009, "Three-Dimensional Finite Element Model of the Cervical Spinal Cord: Preliminary Results of Injury Mechanism Analysis," Spine, **34**(11), pp. 1140–1147.

[19] Persson, C., Summers, J., and Hall, R. M., 2011, "The Importance of Fluid-Structure Interaction in Spinal Trauma Models," J. Neurotrauma, **28**(1), pp. 113–125.
[20] Khuyagbaatar, B., Kim, K., and Kim, Y. H., 2014, "Effects of Bone Fragment Impact on Biomechanical Parameters Related to Spinal Cord Injury: A Finite Element Study," J. Biomech., **47**(11), pp. 2820–2825
[21] Greaves, C. Y., Gadala, M. S., and Oxland, T. R., 2008, "A Three-Dimensional Finite Element Model of the Cervical Spine With Spinal Cord: An Investigation of Three Injury Mechanisms," Ann. Biomed. Eng., **36**(3), pp. 396–405.
[22] Lee, S. H., Im, Y. J., Kim, K. T., Kim, Y. H., Park, W. M., and Kim, K., 2011, "Comparison of Cervical Spine Biomechanics After Fixed- and Mobile-Core Artificial Disc Replacement: A Finite Element Analysis," Spine, **36**(9), pp. 700–708.
[23] Ko, H. Y., Park, J. H., and Baek, S. Y., 2004, "Gross Quantitative Measurements of Spinal Cord Segments in Human," Spinal Cord, **42**(1), pp. 35–40.
[24] Kameyama, T., Hashizume, Y., and Sobeu, G., 1996, "Morphologic Features of the Normal Human Cadaveric Spinal Cord," Spine, **21**(11), pp. 1285–1290.
[25] Holsheimer, J., den Boer, J. A., Struijk, J. J., and Rozeboom, A. R., 1994, "MR Assessment of the Normal Position of the Spinal Cord in the Spinal Canal," Am. J. Neuroradiol., **15**(5), pp. 951–959.
[26] Ichihara, K., Taguchi, T., Shimada, Y., Sakuramoto, I., Kawano, S., and Kawai, S., 2001, "Gray Matter of the Bovine Cervical Spinal Cord is Mechanically More Rigid and Fragile Than the White Matter," J. Neurotrauma, **18**(3), pp. 361–367.
[27] Ogden, R. W., 1972, "Large Deformation Isotropic Elasticity: On the Correlation of Theory and Experiment for Incompressible Rubberlike Solids," Proc. R. Soc. London A, **326**(1567), pp. 565–584.
[28] Persson, C., Evans, S., Marsh, R., Summers, J. L., and Hall, R. M., 2010, "Poisson's Ratio and Strain Rate Dependency of the Constitutive Behavior of Spinal Dura Mater," Ann. Biomed. Eng., **38**(3), pp. 975–983.
[29] Brydon, H. L., Hayward, R., Harkness, W., and Bayston, R., 1995, "Physical Properties of Cerebrospinal Fluid of Relevance to Shunt Function 1: The Effect of Protein Upon CSF Viscosity," Br. J. Neurosurg., **9**(5), pp. 639–644.
[30] Bloomfield, I. G., Johnston, I. H., and Bilston, L. E., 1998, "Effects of Proteins, Blood Cells and Glucose on the Viscosity of Cerebrospinal Fluid," Pediatr. Neurosurg., **28**(5), pp. 246–251.
[31] Wilcox, R. K., Boerger, T. O., Allen, D. J., Barton, D. C., Limb, D., Dickson, R. A., and Hall, R. M., 2003, "A Dynamic Study of Thoracolumbar Burst Fracture," J. Bone Jt. Surg. Am. **85**(11), pp. 2184–2189.
[32] Jones, C. F., Kroeker, S. G., Cripton, P. A., and Hall, R. M., 2008, "The Effect of Cerebrospinal Fluid on the Biomechanics of Spinal Cord: An Ex Vivo Bovine Model Using Bovine and Physical Surrogate Spinal Cord," Spine, **33**(17), pp. E580–E588.
[33] Persson, C., McLure, S. W., Summers, J., and Hall, R. M., 2009, "The Effect of Bone Fragment Size and Cerebrospinal Fluid on Spinal Cord Deformation During Trauma: An Ex Vivo Study," J. Neurosurg. Spine, **10**(4), pp. 315–323.
[34] Wilcox, R. K., Allen, D. J., Hall, R. M., Limb, D., Barton, D. C., and Dickson, R. A., 2004, "A Dynamic Investigation of the Burst Fracture Process Using a Combined Experimental and Finite Element Approach," Eur. Spine J., **13**(6), pp. 481–488.
[35] Meves, R., and Avanzi, O., 2006, "Correlation Among Canal Compromise, Neurologic, Deficit, and Injury Severity in Thoracolumbar Burst Fractures," Spine, **31**(18), pp. 2137–2141.
[36] Aebli, N., Rüegg, T. B., Wicki, A. G., Petrou, N., and Krebs, J., 2013, "Predicting the Risk and Severity of Acute Spinal Cord Injury After a Minor Trauma to the Cervical Spine," Spine J., **13**(6), pp. 597–604.
[37] Ngo, L. M., Aizawa, T., Hoshikawa, T., Tanaka, Y., Sato, T., Ishii, Y., and Kokubun, S., 2012, "Fracture and Contralateral Dislocation of the Twin Facet Joints of the Lower Cervical Spine," Eur. Spine J., **21**(2), pp. 282–288.
[38] Yliniemi, E. M., Pellettiere, J. A., Doczy, E. J., Nuckley, D. J., Perry, C. E., and Ching, R. P., 2009, "Dynamic Tensile Failure Mechanics of the Musculoskeletal Neck Using a Cadaver Model," ASME J. Biomech. Eng., **131**(5), p. 051001.
[39] Kroeker, S. G., and Ching, R. P., 2013, "Coupling Between the Spinal Cord and Cervical Vertebral Column Under Tensile Loading," J. Biomech., **46**(4), pp. 773–779.
[40] Choo, A. M., Liu, J., Liu, Z., Dvorak, M., Tetzlaff, W., and Oxland, T. R., 2009, "Modeling Spinal Cord Contusion, Dislocation, and Distraction: Characterization of Vertebral Clamps, Injury Severities, and Node of Ranvier Deformations," J. Neurosci. Methods, **181**(1), pp. 6–17.
[41] Vaccaro, A. R., Hulbert, J., Patel, A. A., Fisher, C., Dvorak, M., Lehman, R. A., Jr., Anderson, P., Harrop, J., Oner, F. C., Arnold, P., Fehlings, M., Hedlund, R., Madrazo, I., Rechtine, G., Aarabi, B., Shainline, M., and Spine Trauma Study Group, 2007, "The Subaxial Cervical Spine Injury Classification System: A Novel Approach to Recognize the Importance of Morphology, Neurology, and Integrity of the Disco-Ligamentous Complex," Spine, **32**(21), pp. 2365–2374.
[42] Persson, C., Summers, J., and Hall, R. M., 2011, "The Effect of Cerebrospinal Fluid Thickness on Traumatic Spinal Cord Deformation," J. Appl. Biomech., **27**(4), pp. 330–335.
[43] Hung, T. K., and Chang, G. L., 1981, "Biomechanical and Neurological Response of the Spinal Cord of a Puppy to Uniaxial Tension," ASME J. Biomech. Eng., **103**(1), pp. 43–47.
[44] Kim, Y. H., Khuyagbaatar, B., and Kim, K., 2013, "Biomechanical Effects of Spinal Cord Compression Due to Ossification of Posterior Longitudinal Ligament and Ligamentum Flavum: A Finite Element Analysis," Med. Eng. Phys., **35**(9), pp. 1266–1271.
[45] Kato, Y., Kanchiku, T., Imajo, Y., Kimura, K., Ichihara, K., Kawano, S., Hamanaka, D., Yaji, K., and Taguchi, T., 2010, "Biomechanical Study of the Effect of Degree of Static Compression of the Spinal Cord in Ossification of the Posterior Longitudinal Ligament," J. Neurosurg. Spine, **12**(3), pp. 301–305.
[46] Nishida, N., Kato, Y., Imajo, Y., Kawano, S., and Taguchi, T., 2011, "Biomechanical Study of the Spinal Cord in Thoracic Ossification of the Posterior Longitudinal Ligament," J. Spinal Cord Med., **34**(5), pp. 518–522.
[47] Galle, B., Ouyang, H., Shi, R., and Nauman, E., 2010, "A Transversely Isotropic Constitutive Model of Excised Guinea Pig Spinal Cord White Matter," J. Biomech., **43**(14), pp. 2839–2843.
[48] Sparrey, C. J., and Keaveny, T. M., 2011, "Compression Behavior of Porcine Spinal Cord White Matter," J. Biomech., **44**(6), pp. 1078–1082.